Influence of Preparation Condition on the Performance of Ni-based Catalysts for the Glycerol Steam Reforming

XIE Shuang[1], Zhang Xianghua[2], Tu Qiang[2], Shi Biao[2], Cui Yuehua[2], Chen Changguo[1]

(1. College of Chemistry and Chemical Engineering, Chongqing University, 400044;
2. Chongqing Institute of Green and Intelligent Technology, Chinese Academy of Sciences, 400714)

Abstract: The effect of preparation condition on the performance of Ni-based catalysts was investigated for the glycerol steam reforming. The $La_{0.7}Ce_{0.3}NiO_3$ mixed oxides were synthesized using different solution concentrations and calcination temperatures by co-precipitation method. BET, ICP, XRD, TPR, FE-SEM, CO_2-TPD, TGA and Raman spectroscopy were used to characterize the catalysts. Including La_2NiO_4 phase at lowest solution concentration, catalyst precursor included $LaNiO_3$ phase instead of La_2NiO_4 at other solution concentrations. At low calcination temperature of 700 °C, it was found that smaller particle size of CeO_2 incorporated more lanthanum, higher surface basicity and $La_2O_2CO_3$ phase could effectively inhibit and eliminate coking leading to the better performance of catalyst.

Key words: Hydrogen production;Ni-based catalysts;Glycerol steam reforming;Coking

0 Introduction

With energy crisis and environmental issues, it is urgent to develop renewable energy resources. Currently the use of biomass to obtain liquid fuels has received much interest, such as biodiesel with similar properties as diesel. Deriving from transesterification by vegetable oils or animal fats reacting with alcohol to produce approximately 10 % (w/w) of crude glycerol, biodiesel as carbon neutral fuel is biodegradable and non-toxic. The profitability of biodiesel depends heavily on the economics of the byproducts. Nowadays, glycerol is used mostly in the pharmaceutical, personal care, food and cleaning industries. Glycerol is employed as a source of renewable hydrogen, which provides a promising solution for the dilemma of surplus glycerol.

Various routes for the preparation hydrogen by glycerol, namely steam reforming [1], autothermal reforming [2,3], partial oxidation [4], aqueous-phase reforming [5, 6], supercritical water reforming [7], have been extensively investigated. The glycerol steam reforming (GSR) has similar catalyst process and technology to those of methanol or ethanol steam reforming and provides higher hydrogen yield at atmospheric pressure [8], so GSR is widely utilized. GSR can be represented by Eqs. (1) and (2):

$$C_3H_8O_3 \rightarrow 3CO + 4H_2 \quad (1)$$

$$CO + H_2O \leftrightarrow CO_2 + H_2 \quad (2)$$

Different methods of process intensification and catalytic materials have been extensively studied for steam reforming. For example, Dou et al. studied several methods of process intensification, such as the sorption-enhanced steam reforming [9], chemical looping steam reforming [10,11] and the sorption-enhanced chemical-looping steam reforming [12].

In GSR, the most investigated materials are Ni-, Pt-, Co- and Ru-based catalysts [13-16], and less researched materials are Rh-, Ir- and Pd-based catalysts [17-20]. As a matter of fact, Ni-based catalysts are less costly and well known to promote the rupture of C-C, O-H, and C-H bonds [21-23]. However, main challenges for Ni-based catalysts are sinter, carbon deposition and rich hydrogen

Foundations: National Natural Science Foundation of China (No.21473180)
Brief author introduction:XIE Shuang（1991）,Female,Graduate student,Catalytic chemistry
Correspondance author: Chen Changguo(1959),Male,Professor,Electrochemistry. E-mail: cgchen@cqu.edu.cn

gas with a low CO concentration. Accordingly, three strategies were presented to address these challenges containing the methodologies for the preparation of highly dispersed nickel catalysts with strong metal-support interaction, the promotion in the mobility of the surface oxygen and then the removal of surface carbon deposition and the process intensification via the situ absorption of CO_2 [24].

Furthermore, perovskite-type mixed oxides have received increasing attention due to its special crystal structure [25-28]. For $LaNiO_3$, the effect of partial substitution of La with a great range of metal cations (Ce, Ca, Sr, Sm, Nd, etc.) was widely investigated [21,29,30].

But less investigations about the effect of preparation conditions on the performance of perovskite-type mixed oxides are found. In this work solution concentration and calcination temperature were studied over a series of $La_{0.7}Ce_{0.3}NiO_3$ mixed oxides prepared by co-precipitation method. Several characterization techniques and online analysis of gas phase products were used to determine the performance of catalysts in GSR.

1 Experimental

1.1 Preparation Method

When the $La_{0.7}Ce_{0.3}NiO_3$ mixed oxides were prepared by the co-precipitation method, the molar ratio of 0.7:0.3:1:5 for La^{3+}, Ce^{3+}, Ni^{2+} and $HCO3^{1-}$ was kept constant. Only solution concentration and calcination temperature were varied in the co-precipitation procedure. The specific synthesis procedures were as follows. $La(NO_3)_3{\cdot}6H_2O$ (99.0%, Kelon), $Ce(NO_3)_3{\cdot}6H_2O$ (99.0%, Kelon), $Ni(NO_3)_2{\cdot}6H_2O$ (99.0%, Kelon) were dissolved in distilled water together to receive three different concentrations with 0.03, 0.3 and 3 mol/L. Meanwhile ammonium hydrogen carbonate was dissolved in distilled water to obtain three different concentrations with 0.1, 0.6 and 1.9 mol/L. Then three resulting precipitates obtained by adding corresponding precipitant to nitrate solution were filtered, washed with distilled water and dried at 80 °C for 2 h and at 110 °C for 6 h. After that, the materials were carefully ground in a mortar, and then calcined for 6 h at certain temperature, labeled as L*T*-*x*-*y* (*T* is calcination temperature, *T*=900 °C or 700 °C, *x* is concentration of nitrate solution, *x*=0.03, 0.3 and 3 mol/L, *y* is precipitant concentration, *y*=0.1, 0.6 and 1.9 mol/L). Finally, L900-0.03-0.1, L900-0.3-0.6, L900-3-1.9, L700-0.3-0.6, L700-3-1.9 were synthesized.

1.2 Characterization Method

Nitrogen physisorption measurements were conducted utilizing a surface area analyzer (Blesorp-max). Catalysts were degassed at 350 °C for 4 h before N_2 adsorption-desorption measurements. Textural properties of catalysts were obtained by the BET and BJH methods.

After microwave digestion of reduced samples in aqua regia, nickel content was determined by Inductively Coupled Plasma Atomic Emission Spectroscopy (ICP-AES, Agilent 7700x).

The X-ray diffraction (XRD) data were collected using an X'Pert3 Powder Diffractometer operated at 40 kV and 40 mA with Cu Kα radiation (λ=0.154 nm). The Scherrer equation was used to calculate the mean Ni crystal size based on the diffraction peak of Ni (111) facet.

The reducibility of catalyst precursor was evaluated by temperature-programmed reduction (TPR) using a 6 vol% H_2/Ar flow. 30 mg of sample in a U-shaped quartz tube was heated up from 50 °C to 900 °C at a heating rate of 10 °C/min.

Surface basicity of reduced catalyst was measured by the CO_2-temperature programmed desorption (CO_2-TPD). 50 mg of catalyst was reduced at 650 °C for 30 min, followed by flushing with 50 ml/min Ar for 30 min at 650 °C and then cooling down. A 10 vol% CO_2/Ar flow (50

ml/min) was adsorbed at 50 °C for 1 h, and then the sample was purged by 50 ml/min Ar for 30 min. Finally, the TPD of CO_2 was performed from 50 °C to 700 °C at a heating rate of 10 °C/min in an Ar flow (50 ml/min).

Thermal gravity analysis (TGA, STAR^e System METTLERTOLEDO Corp.) was used to investigate the carbon deposition of used catalyst. The catalyst was pretreated at 800 °C for 30 min and then cooled to room temperature in 50 ml/min N_2. Nextly, the catalyst was heated from room temperature to 900 °C at a heating rate of 10 °C/min in 50 ml/min air.

Raman spectroscopy was used to characterize the carbon deposition of 10 mg of used catalyst. Raman spectra were collected using an inVia Raman Microscope (inVia reflex) with a He-Ne green laser (532.14 nm) at ambient conditions in the range of 1000-2000 cm^{-1}.

1.3 Catalysis Measurement

The catalytic tests were investigated in a quartz fixed-bed reactor (inner diameter 8 mm) loaded with 100 mg of powder catalyst. Prior to starting a test, catalyst was reduced in situ at 650 °C under a 5 vol% H_2/N_2 flow (30 ml/min) for 40 min. The feed liquid with stream to carbon molar ratio equaling 5 (S/C=5), was fed at 0.012 ml/min through a peristaltic pump at space time of 49.7 gh/mol. Besides, N_2 carrier gas was kept at 30 ml/min by mass flow controller. The products passed through a cold trap for liquid product capture and then a bed of silica gel (16 cm). The gas products were analyzed online by gas chromatographs (Pgeneral GC 1100) equipped with a thermal conductivity detector and a TDX-01 column (80-100 mesh) with N_2 carrier gas. The catalytic performance was evaluated by hydrogen yield (Y_{H2}), glycerol conversion to gaseous products (X_g) and yield of C-containing gas product (Y_i):

$$Y_{H2}\,(\%) = \frac{F_{\mathrm{H_2},out}}{7F_{Glycerol,in}} \cdot 100$$

$$X_g\,(\%) = \frac{F_{\mathrm{c},out}}{3F_{Glycerol,in}} \cdot 100$$

$$Y_i\,(\%) = \frac{moles\,of\,species\,i\,in\,gas\,product}{moles\,of\,c\,atoms\,in\,feed} \cdot 100$$

where i is the CO, CO_2 or CH_4.

2 Results and discussion

2.1 Characterization of Catalyst

The analysis results of ICP-AES and BET are summarized in Table 1. A 6 wt% loading of Ni on L900-0.03-0.1 is much less than that on other catalysts in range of 12-14 wt%, which exhibits that Ni loading decreases dramatically with solution concentration declining to a certain extent. It is found that calcination temperature influences textural properties of catalyst. When catalyst calcined at 700 °C, solution concentration remarkably affects the textural properties. The L700-3-1.9 shows the highest specific surface area, pore volume and pore diameter.

Table 1 The analysis results of BET and ICP-AES

Reduced catalysts	Ni loading (wt%)	Specific surface area (m^2/g)	Pore volume (cm^3/g)	Av. pore diameter (nm)
L900-0.03-0.1	6	13	0.03	3.2
L900-0.3-0.6	12	15	0.03	3.3
L900-3-1.9	13	13	0.03	2.4
L700-0.3-0.6	13	20	0.06	24.4
L700-3-1.9	14	101	0.46	44.2

The XRD patterns of calcined samples are shown in Fig. 1. Perovskite phase and CeO_2 phase shifting to lower Bragg angles due to lanthana doping, were found in all samples without detection of NiO phase, which indicated that the used co-preparation method was efficient to produce the perovskite structure [21]. The appearance of perovskite structure was not affected by the investigated calcination temperature, which was consistent with the study result of Glisenti et al. [25]. La_2NiO_4 phase (2θ=32.5°) was presented only in L900-0.03-0.1, with $LaNiO_3$ phase (2θ = 23.2°, 32.8°, 47.3°, 58.6°) instead of La_2NiO_4 phase in other catalysts. For preparing catalyst with constant mole numbers of nitrate and precipitant, the formation of La_2NiO_4 requires less nickel than that of $LaNiO_3$. Thus L900-0.03-0.1 had the lowest Ni content in agreement with the ICP result. At low calcination temperature of 700 °C, it was obvious that the diffraction peaks of CeO_2 phase were more diffusive. Smaller particles of CeO_2 possess significantly more Ce^{3+} sites, which contributes to the higher reducibility of the ceria [31].

After reduction treatment (Fig. 2(A) and 2(B)), all catalysts mainly decomposed to Ni (2θ = 44.6°, 51.8°, 76.4°), $La(OH)_3$ (2θ = 15.6°, 27.5°, 39.5°, 48.6°) and CeO_2 with lanthana doping. In Fig. 2B a shift of the diffraction peaks of CeO_2 was larger at calcination temperature of 700 °C, which manifested CeO_2 doping more lanthana. The introduction of other metal cations as dopants (such as La^{3+}) can also modify the oxygen storage capacity (OSC) and surface oxygen mobility (OM) of the oxide by lowering the barrier for oxygen migration and decreasing the activation energy for the reduction of the ceria species [24,32]. Therefore, higher OSC and OM in L700-0.3-0.6 and L700-3-1.9 could only be inferred from the available data. The mean Ni crystal sizes were 11 nm, 11 nm, 12 nm, 13 nm and 13 nm corresponding to L900-0.03-0.1, L900-0.3-0.6, L900-3-1.9, L700-0.3-0.6 and L700-3-1.9, respectively, which revealed that Ni crystal sizes did not have clear correlation with calcination temperature and solution concentration. L900-0.03-0.1 had the weakest intensity of diffraction peak of Ni due to the lowest Ni content as discussed above.

The reduction profiles of catalysts are shown in Fig. 3. The peaks of other catalysts except L900-0.03-0.1 within 300-400 °C and 500-550 °C were defined for the $LaNiO_3$ perovskite-type oxides [21,29], although there were more than three peaks attributing to the fluctuation of TPR system and the reduction of CeO_2 [33]. Reduction peak of L900-0.03-0.1 at highest temperature was ascribed to the existence of La_2NiO_4 [29], which indicated that L900-0.03-0.1 had strongest metal-support interaction (MSI). Moreover, L900-0.03-0.1 had the lowest amount of hydrogen consumption in all samples because of the lowest Ni content (Table 1).

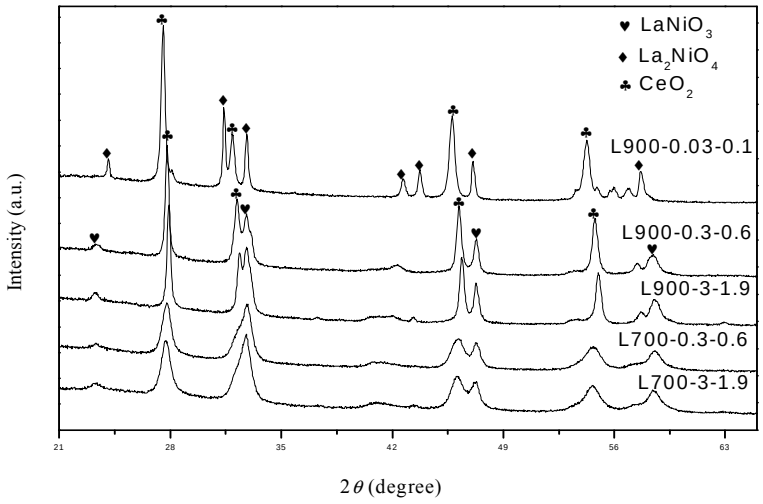

Figure 1 XRD patterns of the $La_{0.7}Ce_{0.3}NiO_3$ perovskite-type mixed oxides

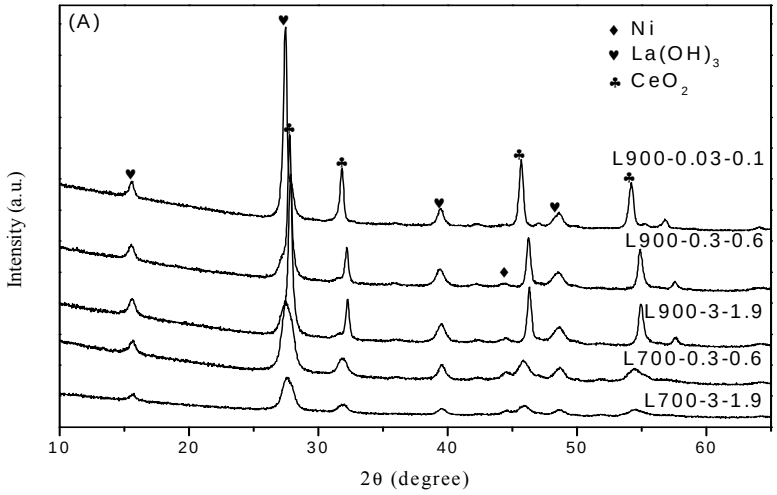

160

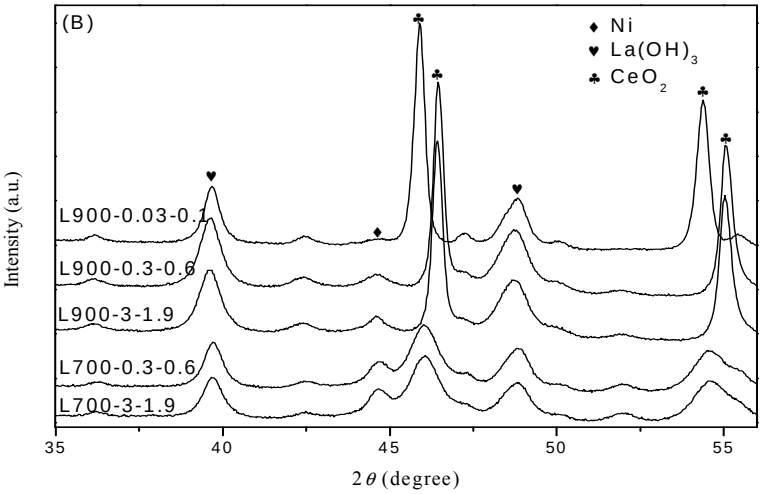

Figure 2 XRD patterns of reduced catalysts

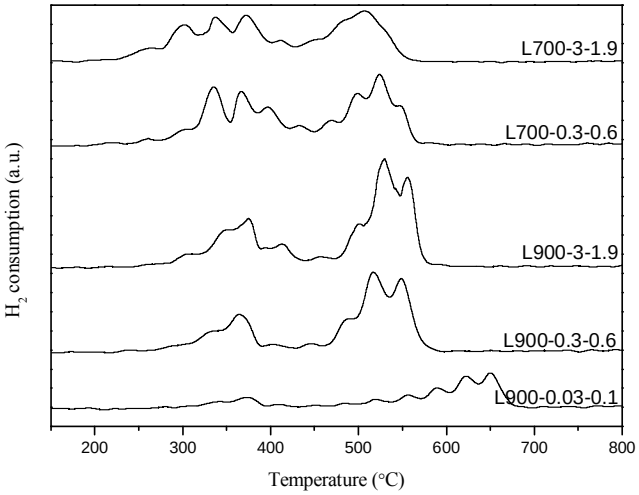

Figure 3 H_2-TPR profiles of the La0.7Ce0.3NiO3 perovskite-type mixed oxides (10 °C/min)

The CO_2-TPD profiles of reduced catalysts are shown in Fig. 4. Two major peaks were observed at 67-152 °C originating from the decomposition of a monodentate carbonate and at 267-647 °C probably arising from the decomposition of bidentate and/or bridged carbonates [34]. It was concluded that calcination temperature and solution concentration could affect surface basic property of catalyst. At calcination temperature of 700 °C, the large amount of strong basic sites of catalysts could be inferred from their high specific surface area. The maximum amount of weak basic sites were obtained, at the highest solution concentration. As solution concentration decreased, strong basic sites of catalyst increased. Charisiou et al. [35] revealed that active sites for the glycerol conversion are not necessarily based on Ni^0, but it is the basicity of the catalysts (oxygen anion sites) which is the key parameter to form acetol and even break C-C bonds to a certain extent. Vizcaíno et al. [36] provided that coke formation from ethylene decreased thanks to the basic properties of Ca/SBA-15 and Mg/SBA-15 supports. Ali Zadeh Sahraei et al. [1] concluded that the enhanced steam adsorption in presence of basic material could also help the oxidation of carbonaceous deposits.

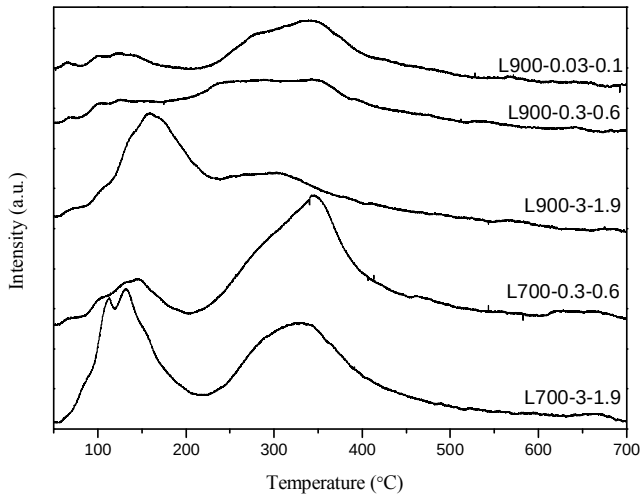

Figure 4 CO_2-TPD curves of reduced catalysts

2.2 Catalysis Performance

The catalytic performance was investigated at 575 °C for GSR with S/C = 5 after 2.5 h of feeding in all samples. The blank experiment in the absence of catalyst was run under the same conditions to observe that hydrogen product was negligible. In addition, The C_2H_4 and C_2H_6 were not detected in all experiments. The yield of gas product and X_g are given in Fig. 5. The CH_4 yield was about 2 % for all samples, which indicated that hydrogenation reactions between CO/CO_2 and H_2 formed were inhibited [37]. The molar CO/CO_2 ratio was about 0.5 on L900-0.03-0.1, while the ratio was approximately 0.2 on other samples. This result illustrated that all catalysts facilitated the water-gas-shift reaction (WGSR). The L900-0.03-0.1 had relatively lower molar CO/CO_2 ratio might due to different catalyst precursor. The H_2 yields were 57 %, 79 %, 82 %, 82 % and 91 % corresponding to L900-0.03-0.1, L900-0.3-0.6, L900-3-1.9, L700-0.3-0.6 and L700-3-1.9, respectively. The X_g were 60 %, 92 %, 88 %, 95 % and 100 %, respectively. The L700-3-1.9 with the highest Ni content and specific surface area had the highest initial H_2 yield and X_g. L900-0.03-0.1 with the minimum Ni content had the lowest initial H_2 yield and X_g. The result elucidated that catalytic activity positively correlated with primary Ni content and specific surface area, but was unrelated to the particle size of Ni.

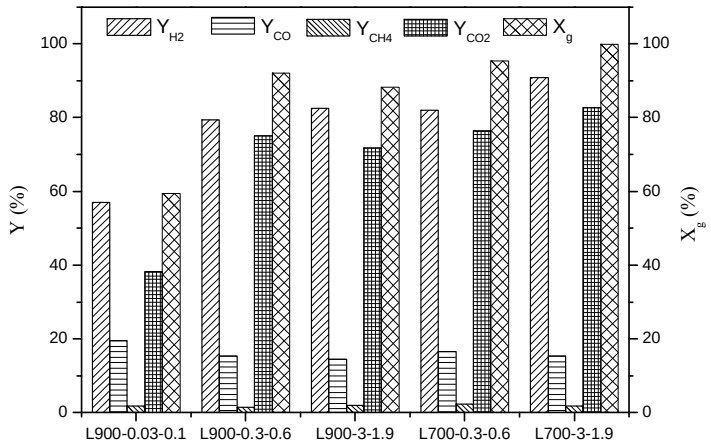

Figure 5 The yield of gas product and *X*g for all samples in GSR after 2.5 h of feeding
Reaction condition: T = 575 °C, S/C = 5 and W/F = 49.7 gh/mol

Stability texts of catalysts with similar Ni content were performed for 21.5 h. The yield of gas product and X_g are displayed in Fig. 6. There is always a gap between data obtained after 10.5 h and 20 h in Fig. 7, because the data were not collected at night. The average CH_4 yield was near 2 %, and the average molar CO/CO_2 ratio was about 0.3 in all catalysts. Hence, the prepared catalysts could hinder methanation reaction and promote WGSR. The H_2 yield declined smoothly from 80 % to 66 %, and X_g decreased from 92 % to 70 % for L900-0.3-0.6 during stability experiment. There was a rapid decline in H_2 yield from 82 % to 44 %, and X_g had the same change trend for L900-3-1.9. After the H_2 yield reduced from 82 % to 70 % within the initial 4.5 h, the H_2 yield was basically stable at around 70 % for L700-0.3-0.6. Meanwhile the same change trend was observed in X_g. There were rapid decreases in H_2 yield from 91 % to 60 % and in X_g from 100% to 61 % during 21.5 h for L700-3-1.9. Furthermore the reductions of H_2 yield and X_g were extremely slow after 9.5 h.

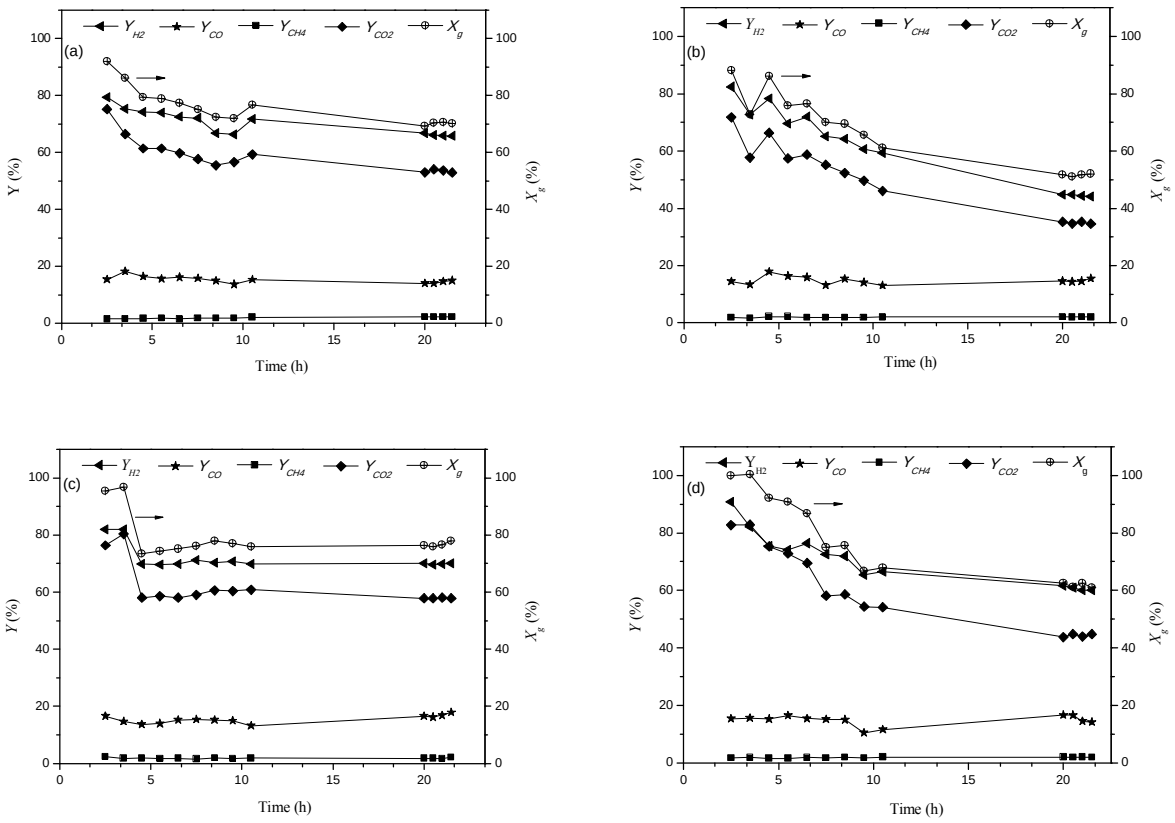

Figure 6 Stability tests of all catalysts in GSR (Reaction condition: T = 575 °C, S/C= 5 and W/F = 49.7 gh/mol)
(a) L900-0.3-0.6, (b) L900-3-1.9, (c) L700-0.3-0.6, (d) L700-3-1.9

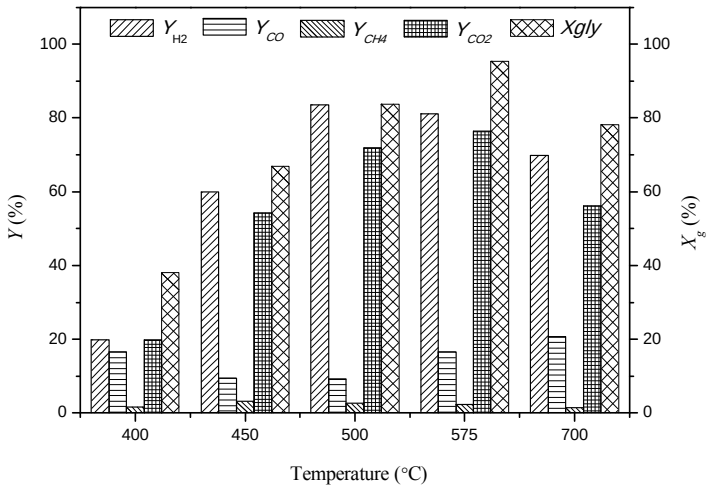

Figure 7 The yield of gas product and *X*g over the L700-0.3-0.6 after 3 h of feeding in GSR
(Reaction condition: T = 400 °C, 450 °C, 500 °C, 575 °C and 700 °C, S/C = 5 and W/F = 49.7 gh/mol

Reaction temperature from 400 to 700 °C was studied after 3 h of feeding over L700-0.3-0.6 with the best performance. The experiment result is illustrated in Fig. 7. X_g increased with increasing temperature below 575 °C and it underwent a drop from 575 °C to 700 °C. H_2 yield raised with increasing temperature below 500 °C, and it underwent a drop from 500 °C to 700 °C; H_2 yields at 500 °C and 575 °C were rather close. Possible explanations for the above results were

the C-C bond cleavage favored at higher temperatures, the thermodynamic equilibrium and carbon deposits [22,30,38,39] . CH_4 yield was very low over the whole temperature range, which clarified that the prepared catalyst had a sufficient capacity for reforming CH_4 into hydrogen and carbon oxide [35,40, 41]. It was worth notice that H_2 yield could reach around 60 % at 450 °C.

2.3 Characterization of Used Catalyst

The XRD patterns (Fig. 8) show main phases of all used catalysts including Ni, $La_2O_2CO_3$ (2θ = 11.1°, 22.2°, 25.8°, 30.3°, 44.4°) and CeO_2 with lanthana doping. It was only inferred from the available data that the appearance of $La_2O_2CO_3$ phase rather than $La(OH)_3$ phase was assigned to the existence of CO_2 at reaction condition [29, 42, 43] . Verykios et al. [44] discovered that catalytic activity occurs at the Ni-$La_2O_2CO_3$ interface, while the oxycarbonate species participate directly by reacting with deposited carbon, thus restoring the activity of the Ni sites at the interface. Simultaneously, de Lima et al. [26] reported that $La_2O_2CO_3$ strongly interacts with Ni particles, inhibiting sintering during reaction. The lines of Ni phase overlap with those of $La_2O_2CO_3$ phase, thus it is difficult to estimate the particle size of Ni on used samples.

The Raman spectroscopy of used catalyst (Fig. 9) is given to characterize the structure of deposited coke after stability tests. All samples had two characteristic peaks located at around 1338 cm^{-1} (D band) and 1587 cm^{-1} (G band) usually assigned to phonons of E_{2g} and A_{1g} symmetry, respectively [45-47] . It was obvious that D band area was greater than G band area, which indicated a predominance of a low degree of crystalline carbon species in all samples.

Additionally, the deposited carbon was determined by TGA. The derivative thermograms are shown in Fig. 10. In order to exclude the influence of $La_2O_2CO_3$, all samples were pretreated at 800 °C for 30 min, the mass losses were 3.2 %, 3.5 %, 4.3 % and 4.0 % corresponding to L900-0.3-0.6, L900-3-1.9, L700-0.3-0.6 and L700-3-1.9, respectively. In Fig. 10 the slight mass gain of L900-3-1.9 was observed, while other catalysts had obvious increments in mass, with the maximum mass reaching at 403 °C for all catalysts. The result could be due to the oxidations of metal nickel and Ce^{3+} [22,48]. Different carbon types were obtained for each catalyst, because of amorphous carbon oxidizing below 550 °C and the oxidation of graphitic/filamentous carbon required higher temperature [49,50]. The mass of carbon deposition was represented by the difference between the maximum mass due to oxidation and the minimum mass. Thereby the mass loss due to carbon deposition followed the order, L700-0.3-0.6 (9.9 %) < L700-3-1.9 (13.9 %) < L900-3-1.9 (19.7 %) < L900-0.3-0.6 (22.4 %). The CO, CH_4, and C2 species were the initiating species of the coke deposited as some of them underwent a further Boudouard reaction, methane decomposition, and polymerization, respectively, forming different coke species on the catalyst surface [23]. Furthermore, CO_2-TPD indicated that surface basicity of catalysts followed the order L900-0.3-0.6 < L900-3-1.9 < L700-0.3-0.6 < L700-3-1.9, and surface basicity of L700-0.3-0.6 was slightly lower than that of L700-3-1.9. Therefore, L700-0.3-0.6 had the lowest coking amount contributed to high basic site density, highest $La_2O_2CO_3$ mass, CeO_2 with more lanthana doping and smaller particle size of CeO_2. L900-0.3-0.6 had the highest coking amount ascribed to the lowest basic site density and $La_2O_2CO_3$ mass. While there was still high H_2 yield (66 %) for L900-0.3-0.6 after 21.5 h of reaction. This result could be due to most carbonaceous species covering the surface of supports rather than Ni active centers. The coking was mainly influenced by surface basicity of catalyst and mass of $La_2O_2CO_3$ in this work, but the coking was significantly associated with particle size of Ni in other literatures [29,51].

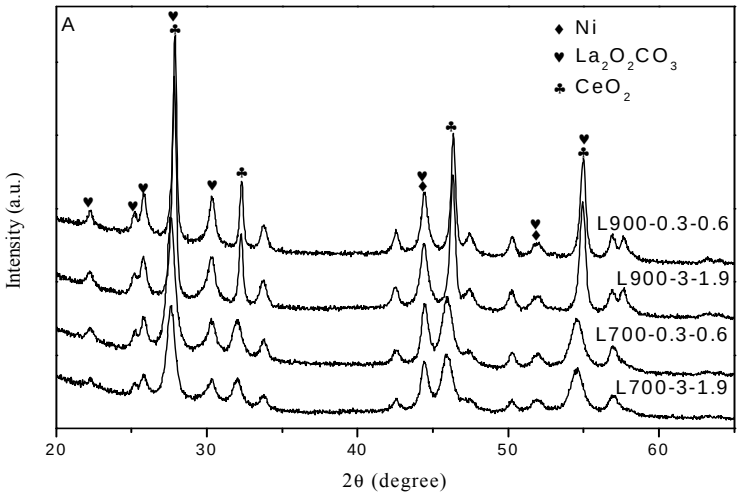

Figure 8 XRD patterns of used catalysts after stability tests

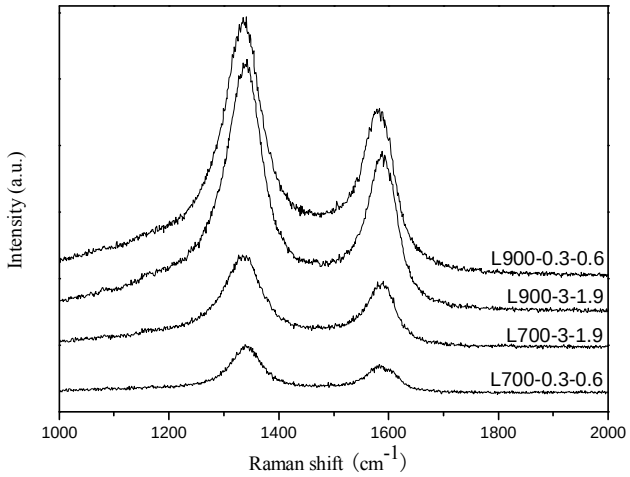

Figure 9 Raman spectra of used catalysts after stability tests

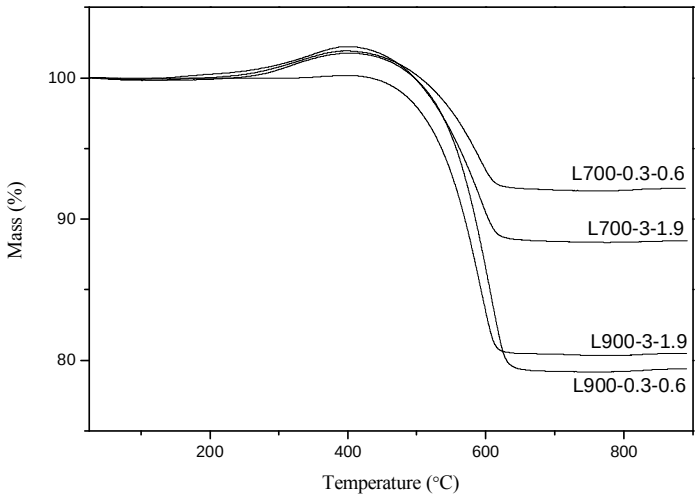

Figure 10 TGA curves for used catalysts after stability tests

3 Conclusion

In this work, solution concentration and calcination temperature could influence physicochemical, structural and textural properties of the synthesized catalysts. L900-0.03-0.1 with the lowest Ni content had the lowest initial activity, so the decline in solution concentration to a certain extent was adverse to nickel deposing. L700-3-1.9 had excellent initial activity contributed to the highest Ni content and specific surface area. L700-0.3-0.6 exhibited optimal catalytic performance, because of the lowest coking content due to the highest $La_2O_2CO_3$ mass, high density of basic sites and small particle size of CeO_2 doping more lanthana. Hence proper solution concentration and low calcination temperature induced great catalytic performance for glycerol steam reforming.

Acknowledgements

This work is supported by National Natural Science Foundation of China under grant number 21473180.

References

[1] ALI ZADEH SAHRAEI O, LARACHI F, ABATZOGLOU N, ILIUTA M C. Hydrogen production by glycerol steam reforming catalyzed by Ni-promoted Fe/Mg-bearing metallurgical wastes[J]. Applied Catalysis B: Environmental, 2017, 219: 183-193.
[2] WANG S, WANG Q, SONG X, CHEN J. Dry autothermal reforming of glycerol with in situ hydrogen separation via thermodynamic evaluation[J]. International Journal of Hydrogen Energy, 2017, 42 (2): 838-847.
[3] LEAL A L, SORIA M A, MADEIRA L M. Autothermal reforming of impure glycerol for H 2 production: Thermodynamic study including in situ CO 2 and/or H 2 separation[J]. International Journal of Hydrogen Energy, 2016, 41 (4): 2607-2620.
[4] WANG W. Thermodynamic analysis of glycerol partial oxidation for hydrogen production[J]. Fuel Processing Technology, 2010, 91 (11): 1401-1408.
[5] EL DOUKKALI M, IRIONDO A, MILETIC N, CAMBRA J F, ARIAS P L. Hydrothermal stability improvement of NiPt-containing γ-Al 2 O 3 catalysts tested in aqueous phase reforming of glycerol/water mixture for H 2 production[J]. International Journal of Hydrogen Energy, 2017, 42 (37): 23617-23630.
[6] SUBRAMANIAN N D, CALLISON J, CATLOW C R A, WELLS P P, DIMITRATOS N. Optimised hydrogen production by aqueous phase reforming of glycerol on Pt/Al 2 O 3[J]. International Journal of Hydrogen Energy, 2016, 41 (41): 18441-18450.
[7] GUTI RREZ ORTIZ F J, CAMPANARIO F J, AGUILERA P G, OLLERO P. Supercritical water reforming of glycerol: Performance of Ru and Ni catalysts on Al2O3 support[J]. Energy, 2016, 96: 561-568.
[8] MANFRO R L, SOUZA M M V M. Production of Renewable Hydrogen by Glycerol Steam Reforming Using Ni-Cu-Mg-Al Mixed Oxides Obtained from Hydrotalcite-like Compounds[J]. Catalysis Letters, 2014, 144 (5): 867-877.
[9] DOU B, JIANG B, SONG Y, ZHANG C, WANG C, CHEN H, DU B, XU Y. Enhanced hydrogen production by sorption-enhanced steam reforming from glycerol with in-situ CO 2 removal in a fixed-bed reactor[J]. Fuel, 2016, 166: 340-346.
[10] JIANG B, DOU B, WANG K, SONG Y, CHEN H, ZHANG C, XU Y, LI M. Hydrogen production from chemical looping steam reforming of glycerol by Ni based Al-MCM-41 oxygen carriers in a fixed-bed reactor[J]. Fuel, 2016, 183: 170-176.
[11] JIANG B, DOU B, SONG Y, ZHANG C, DU B, CHEN H, WANG C, XU Y. Hydrogen production from chemical looping steam reforming of glycerol by Ni-based oxygen carrier in a fixed-bed reactor[J]. Chemical Engineering Journal, 2015, 280: 459-467.
[12] DOU B, SONG Y, WANG C, CHEN H, YANG M, XU Y. Hydrogen production by enhanced-sorption chemical looping steam reforming of glycerol in moving-bed reactors[J]. Applied Energy, 2014, 130: 342-349.
[13] CARRERO A, VIZCA NO A J, CALLES J A, GARC A-MORENO L. Hydrogen production through glycerol steam reforming using Co catalysts supported on SBA-15 doped with Zr, Ce and La[J]. Journal of Energy Chemistry, 2017, 26 (1): 42-48.
[14] MENOR M, SAYAS S, CHICA A. Natural sepiolite promoted with Ni as new and efficient catalyst for the sustainable production of hydrogen by steam reforming of the biodiesel by-products glycerol[J]. Fuel, 2017, 193: 351-358.
[15] SOARES R R, MARTINS D F, PEREIRA D E S, ALMEIDA M B, LAM Y L. On the gas-phase reforming of glycerol by Pt on carbon black: Effects of metal particle size and pH value of the glycerol stream[J]. Journal of Molecular Catalysis A: Chemical, 2016, 422: 142-147.

[16] T L M M, ARAQUE M, CENTENO M A, ROGER A C. Role of ruthenium on the catalytic properties of CeZr and CeZrCo mixed oxides for glycerol steam reforming reaction toward H2 production[J]. Catalysis Today, 2015, 242: 80-90.
[17] ARAQUE M, MART NEZ T L M, VARGAS J C, CENTENO M A, ROGER A C. Effect of the active metals on the selective H2 production in glycerol steam reforming[J]. Applied Catalysis B: Environmental, 2012, 125: 556-566.
[18] MART NEZ T L M, ARAQUE M, VARGAS J C, ROGER A C. Effect of Ce/Zr ratio in CeZr-CoRh catalysts on the hydrogen production by glycerol steam reforming[J]. Applied Catalysis B: Environmental, 2013, 132-133: 499-510.
[19] HUANG X, DANG C, YU H, WANG H, PENG F. Morphology Effect of Ir/La2O2CO3Nanorods with Selectively Exposed {110} Facets in Catalytic Steam Reforming of Glycerol[J]. ACS Catalysis, 2015, 5 (2): 1155-1163.
[20] EBSHISH A, YAAKOB Z, TAUFIQ-YAP Y H, BSHISH A, SHAIBANI A. Catalytic Steam Reforming of Glycerol Over Cerium and Palladium-Based Catalysts for Hydrogen Production[J]. Journal of Fuel Cell Science and Technology, 2013, 10 (2): 021003.
[21] FRANCHINI C A, ARANZAEZ W, DUARTE DE FARIAS A M, PECCHI G, FRAGA M A. Ce-substituted LaNiO3 mixed oxides as catalyst precursors for glycerol steam reforming[J]. Applied Catalysis B: Environmental, 2014, 147: 193-202.
[22] WU G, ZHANG C, LI S, HAN Z, WANG T, MA X, GONG J. Hydrogen Production via Glycerol Steam Reforming over Ni/Al2O3: Influence of Nickel Precursors[J]. ACS Sustainable Chemistry & Engineering, 2013, 1 (8): 1052-1062.
[23] KAMONSUANGKASEM K, THERDTHIANWONG S, THERDTHIANWONG A, THAMMAJAK N. Remarkable activity and stability of Ni catalyst supported on CeO 2 -Al 2 O 3 via CeAlO 3 perovskite towards glycerol steam reforming for hydrogen production[J]. Applied Catalysis B: Environmental, 2017, 218: 650-663.
[24] LI S, GONG J. Strategies for improving the performance and stability of Ni-based catalysts for reforming reactions[J]. Chemical Society reviews, 2014, 43 (21): 7245-56.
[25] GLISENTI A, GALENDA A, NATILE M M. Steam reforming and oxidative steam reforming of methanol and ethanol: The behaviour of LaCo0.7Cu0.3O3[J]. Applied Catalysis A: General, 2013, 453: 102-112.
[26] DE LIMA S M, DA SILVA A M, DA COSTA L O O, ASSAF J M, MATTOS L V, SARKARI R, VENUGOPAL A, NORONHA F B. Hydrogen production through oxidative steam reforming of ethanol over Ni-based catalysts derived from La1−xCexNiO3 perovskite-type oxides[J]. Applied Catalysis B: Environmental, 2012, 121-122: 1-9.
[27] PERE GUEZ R, GONZ LEZ-DELACRUZ V M, HOLGADO J P, CABALLERO A. Synthesis and characterization of a LaNiO3 perovskite as precursor for methane reforming reactions catalysts[J]. Applied Catalysis B: Environmental, 2010, 93 (3-4): 346-353.
[28] CHEN S Q, WANG H, LIU Y. Perovskite La-St-Fe-O (St=Ca, Sr) supported nickel catalysts for steam reforming of ethanol: The effect of the A site substitution[J]. International Journal of Hydrogen Energy, 2009, 34 (19): 7995-8005.
[29] WU G, LI S, ZHANG C, WANG T, GONG J. Glycerol steam reforming over perovskite-derived nickel-based catalysts[J]. Applied Catalysis B: Environmental, 2014, 144: 277-285.
[30] CUI Y, GALVITA V, RIHKO-STRUCKMANN L, LORENZ H, SUNDMACHER K. Steam reforming of glycerol: The experimental activity of La1−xCexNiO3 catalyst in comparison to the thermodynamic reaction equilibrium[J]. Applied Catalysis B: Environmental, 2009, 90 (1-2): 29-37.
[31] SOYKAL I I, SOHN H, SINGH D, MILLER J T, OZKAN U S. Reduction Characteristics of Ceria under Ethanol Steam Reforming Conditions: Effect of the Particle Size[J]. ACS Catalysis, 2014, 4 (2): 585-592.
[32] PAIER J, PENSCHKE C, SAUER J. Oxygen defects and surface chemistry of ceria: quantum chemical studies compared to experiment[J]. Chemical reviews, 2013, 113 (6): 3949-85.
[33] DUARTE DE FARIAS A M, NGUYEN-THANH D, FRAGA M A. Discussing the use of modified ceria as support for Pt catalysts on water-gas shift reaction[J]. Applied Catalysis B: Environmental, 2010, 93 (3-4): 250-258.
[34] EBSHISH A, YAAKOB Z, TAUFIQ-YAP Y, BSHISH A. Investigation of the Process Conditions for Hydrogen Production by Steam Reforming of Glycerol over Ni/Al2O3 Catalyst Using Response Surface Methodology (RSM)[J]. Materials, 2014, 7 (3): 2257-2272.
[35] CHARISIOU N D, SIAKAVELAS G, PAPAGERIDIS K N, BAKLAVARIDIS A, TZOUNIS L, POLYCHRONOPOULOU K, GOULA M A. Hydrogen production via the glycerol steam reforming reaction over nickel supported on alumina and lanthana-alumina catalysts[J]. International Journal of Hydrogen Energy, 2017, 42 (18): 13039-13060.
[36] VIZCA NO A J, CARRERO A, CALLES J A. Comparison of ethanol steam reforming using Co and Ni catalysts supported on SBA-15 modified by Ca and Mg[J]. Fuel Processing Technology, 2016, 146: 99-109.
[37] PASTOR-P REZ L, SEP LVEDA-ESCRIBANO A. Low temperature glycerol steam reforming on bimetallic PtSn/C catalysts: On the effect of the Sn content[J]. Fuel, 2017, 194: 222-228.
[38] CHIODO V, FRENI S, GALVAGNO A, MONDELLO N, FRUSTERI F. Catalytic features of Rh and Ni supported catalysts in the steam reforming of glycerol to produce hydrogen[J]. Applied Catalysis A: General, 2010, 381 (1-2): 1-7.
[39] DAVDA R R, SHABAKER J W, HUBER G W, CORTRIGHT R D, DUMESIC J A. A review of catalytic issues and process conditions for renewable hydrogen and alkanes by aqueous-phase reforming of oxygenated hydrocarbons over supported metal catalysts[J]. Applied Catalysis B: Environmental, 2005, 56 (1-2): 171-186.

[40] CHARISIOU N D, PAPAGERIDIS K N, SIAKAVELAS G, TZOUNIS L, KOUSI K, BAKER M A, HINDER S J, SEBASTIAN V, POLYCHRONOPOULOU K, GOULA M A. Glycerol Steam Reforming for Hydrogen Production over Nickel Supported on Alumina, Zirconia and Silica Catalysts[J]. Topics in Catalysis, 2017, 60 (15-16): 1226-1250.
[41] CHEN S Q, LIU Y. LaFeyNi1−yO3 supported nickel catalysts used for steam reforming of ethanol[J]. International Journal of Hydrogen Energy, 2009, 34 (11): 4735-4746.
[42] BATIOT-DUPEYRAT C, GALLEGO G A S, MONDRAGON F, BARRAULT J, TATIBOU T J-M. CO2 reforming of methane over LaNiO3 as precursor material[J]. Catalysis Today, 2005, 107-108: 474-480.
[43] SIERRA GALLEGO G, MONDRAG N F, TATIBOU T J-M, BARRAULT J, BATIOT-DUPEYRAT C. Carbon dioxide reforming of methane over La2NiO4 as catalyst precursor-Characterization of carbon deposition[J]. Catalysis Today, 2008, 133-135: 200-209.
[44] VERYKIOS X. Catalytic dry reforming of natural gas for the production of chemicals and hydrogen[J]. Chem. Ind., 2002, 56: 238-255.
[45] BOBADILLA L F, ÁLVAREZ A, DOM NGUEZ M I, ROMERO-SARRIA F, CENTENO M A, MONTES M, ODRIOZOLA J A. Influence of the shape of Ni catalysts in the glycerol steam reforming[J]. Applied Catalysis B: Environmental, 2012, 123-124: 379-390.
[46] SADANANDAM G, RAMYA K, KISHORE D B, DURGAKUMARI V, SUBRAHMANYAM M, CHARY K V R. A study to initiate development of sustainable Ni/γ-Al2O3 catalyst for hydrogen production from steam reforming of biomass-derived glycerol[J]. RSC Adv., 2014, 4 (61): 32429-32437.
[47] BOBADILLA L F, ROMERO-SARRIA F, CENTENO M A, ODRIOZOLA J A. Promoting effect of Sn on supported Ni catalyst during steam reforming of glycerol[J]. International Journal of Hydrogen Energy, 2016, 41 (22): 9234-9244.
[48] GO Y-J, GO G-S, LEE H-J, MOON D-J, PARK N-C, KIM Y-C. The relation between carbon deposition and hydrogen production in glycerol steam reforming[J]. International Journal of Hydrogen Energy, 2015, 40 (35): 11840-11847.
[49] CALLES J A, CARRERO A, VIZCA NO A J, GARC A-MORENO L. Hydrogen production by glycerol steam reforming over SBA-15-supported nickel catalysts: Effect of alkaline earth promoters on activity and stability[J]. Catalysis Today, 2014, 227: 198-206.
[50] IRIONDO A, BARRIO V L, CAMBRA J F, ARIAS P L, GUEMEZ M B, SANCHEZ-SANCHEZ M C, NAVARRO R M, FIERRO J L G. Glycerol steam reforming over Ni catalysts supported on ceria and ceria-promoted alumina[J]. International Journal of Hydrogen Energy, 2010, 35 (20): 11622-11633.
[51] VIZCA NO A J, CARRERO A, CALLES J A. Ethanol steam reforming on Mg- and Ca-modified Cu–Ni/SBA-15 catalysts[J]. Catalysis Today, 2009, 146 (1-2): 63-70.

制备条件对甘油蒸气重整中镍基催化剂性能的影响

谢爽[1]，张向华[2]，涂强[2]，石彪[2]，崔月华[2]，陈昌国[1]
（1. 重庆大学化学化工学院，400044；
2. 中国科学院重庆绿色智能技术研究院，400714）

摘要：研究了制备条件对甘油蒸气重整中镍基催化剂性能的影响。在不同的溶液浓度和焙烧温度下通过共沉淀法合成 $La_{0.7}Ce_{0.3}NiO_3$ 混合氧化物催化剂。采用 BET、ICP、XRD、TPR、FE-SEM、CO_2-TPD、TGA 和拉曼光谱对催化剂进行了表征。在最低溶液浓度下催化剂前驱体包含 La_2NiO_4 物相，然而在其他溶液浓度下，是 $LaNiO_3$ 物相而不是 La_2NiO_4 物相。在 700℃低的焙烧温度下，发现较小粒径的 CeO_2 且掺入了更多的镧，有更高的表面碱度以及出现 $La_2O_2CO_3$ 物相，能够有效抑制和消除积碳，使得催化剂有更好的性能。

关键词：产氢；镍基催化剂；甘油蒸气重整；积碳
中图分类号：O6